Note: This work has not yet been peer reviewed

Framework for curvilinear catheter implantation in HDR prostate brachytherapy for dominant intraprostatic lesions (DIL) dose escalation – feasibility study

Blayton Padasdao[1], Rex Imanaka[1], Tarun K Podder[2], Bardia Konh[1]

The department and institution to which the work should be attributed: Department of Mechanical Engineering, University of Hawaii at Manoa

Corresponding author: Bardia Konh, Postal Address: 2540 Dole St., Holmes Hall 302, Honolulu, HI 96822, Email Address: konh@hawaii.edu, Telephone Number: 808-956-2142, Facsimile Number: 808-956-2373

Source of financial support: Research reported in this publication was supported by the National Institute Of Biomedical Imaging And Bioengineering of the National Institutes of Health under Award Number K25EB030562. The content is solely the responsibility of the authors and does not necessarily represent the official views of the National Institutes of Health.

Category of the manuscript: Original Article

Word Count: 4815

Numbers of Figures: 11

Numbers of Tables: 4

[1] Department of Mechanical Engineering, University of Hawaii at Manoa, Honolulu, HI 96822, USA
[2] SUNY Upstate Medical University, Syracuse, NY

Abstract

Background

High-dose-rate (HDR) brachytherapy has been recognized as a popular treatment for patients with intermediate- and high-risk prostate cancer, despite its side-effects such as edema, incontinence, and impotence. Dose escalation to dominant intraprostatic lesions (DILs) results in improved cancer control. However, its application is limited due to the risk of excessive irradiation to organs-at-risk (OARs) such as the urethra, bladder, rectum.

Methods

This work introduces curvilinear catheter implantation for dose escalation to the DIL, while reducing toxicity to OARs. Curvilinear catheters were first pre-planned for an anonymized patient using Oncentra treatment planning system (TPS) and hybrid inverse planning optimization (HIPO) algorithm. The curved needles were then analyzed using MATLAB to extract their radius of curvature. Tendon-driven active needles were then used to implant curvilinear catheters inside a patient-specific phantom tissue.

Results

Proposed curvilinear catheter implantation resulted in significant improvement in dosimetric plans. Tendon-driven active needles were shown to be capable of realizing required pre-planned curvatures inside prostate. Accuracy of needle implantation was evaluated and reported.

Conclusions

This work demonstrates the feasibility of using tendon-driven active needles in curvilinear catheter implantation inside prostate to improve the outcomes of HDR-BT via dose escalation to the DILs and radiation dose reduction to the OARs.

Keywords:

Curvilinear catheter implantation, dose escalation, dominant intraprostatic lesions, reduced toxicity to organs at risk, improved clinical outcome

1. Introduction

Prostate cancer is the second most common cancer in the U.S. with an estimated 288,300 new cases and 34,700 deaths in 2023 [1]. High-dose-rate (HDR) brachytherapy (BT), which entails delivery of temporary high-dose radiation to the prostate gland to eradiate cancer [2], has been identified as one of the most effective treatment modalities [3]. HDR-BT involves implantation of 15 to 20 straight catheters inside prostate to provide access channels to place a radiation source (e.g., iridium-192 capsule is welded at the end of a steel wire) at desired positions (known as dwell positions). In current practice, the catheter implantation is done manually using transrectal ultrasound (TRUS) guidance. Upon catheter implantation, a CT scan is taken to provide a 3D image of the implanted catheters with respect to the prostate and the organs at risk (OARs) such as urethra, bladder, and rectum. As an alternative, both the catheter placement and treatment can be done with TRUS guidance, i.e., without the CT images. Dosimetric planning is done at this point to determine dwell positions and estimate dwell time (radiation period) based on the actual position of the catheters and prescribed radiation dose. An afterloader device is then used to position the radiation source at dwell positions for their respective dwell time based on the dosimetric plan. The afterloader device retracts the radiation source from the patient after the treatment delivery.

Conventional rigid needles and templates only allow insertions only in a straight trajectory, with no conformity to the patient's specific anatomy. Studies have reported that the existing BT procedures can result in side-effects such as edema, incontinence, and impotence resulted by an excessive dose to the OARs [4]. Imprecise catheter implantation often causes insufficient dose to the cancer and/or inadvertent radiation of the OARs. The former causes failure of treatment, while the latter results in adverse side effects like rectal ulceration, incontinence, and dysuria (painful urination). Studies have also shown improved outcomes (e.g., cancer control 8-year biochemical failure free survival) upon boost doses to dominant intraprostatic lesions (DILs) [5,6]. Prostate BT provides unique opportunity to escalate dose to the DILs, however, bounded due to the high risk of intoxicating the OARs.

The curvilinear catheters implantation, which is conformal to the patient-specific anatomy, provides access channels away from the OARs and closer to the DILs to optimize dosimetry and expand the limits for dose escalation to the DILs. In a previous study with 20 patients [7], we showed that the curvilinear catheter implantation yields significantly improved dosimetric plans with a substantial reduction in number of needles compared to conventional rectilinear (straight) catheter implantation. The study showed a high potential to improve the clinical outcomes for prostate cancer patients. This work presents the feasibility of curvilinear catheter implantation method using tendon-driven active needles, along with a framework to realize the plan inside a patient-specific phantom tissue.

This work is organized as follows: Section 2 introduces a framework for curvilinear catheter implantation. Section 2.1.1 pre-plans a curvilinear catheter implantation and a dosimetric plan for an anonymized patient, while Section 2.1.2 evaluates the dosimetric plan. Section 2.2.1 analyzes the catheters' curvatures for the implantation. Section 2.2.2 introduces a new design of tendon-driven active needles to realize the required curvatures. Section 2.2.3 presents our robotic system to insert and actuate the active needles. Section 2.3.1 presents a patient-specific phantom tissue, specifically developed to evaluate the active needles as explained in Section 2.3.2. Section 3.1 presents the dosimetric benefits of using curvilinear catheters in HDR BT. Sections 3.2 and 3.3 demonstrate the feasibility of curvilinear catheter implantation inside prostate via evaluations in air and inside a phantom tissue, respectively.

2. Materials and Methods

Figure 1 shows a framework to realize curvilinear catheter implantation inside prostate gland for HDT BT that includes: (i) identification of patient-specific organs of patient from MRI and/or CT scans, (ii) manual mapping of curved trajectories inside the prostate gland conformal to the prostate boundaries and away from the OARs, (iii) estimation of dosimetric benefits, (iv) identification of best planar polynomial fit to the curved trajectories, (v) design and development of a tendon-driven active needle to realize the objective curvatures, (vi) design and development of a custom template for proper angulation of the needles, and (vii) evaluation of the plan in air and inside patient-specific phantom tissue with actual geometric relationships.

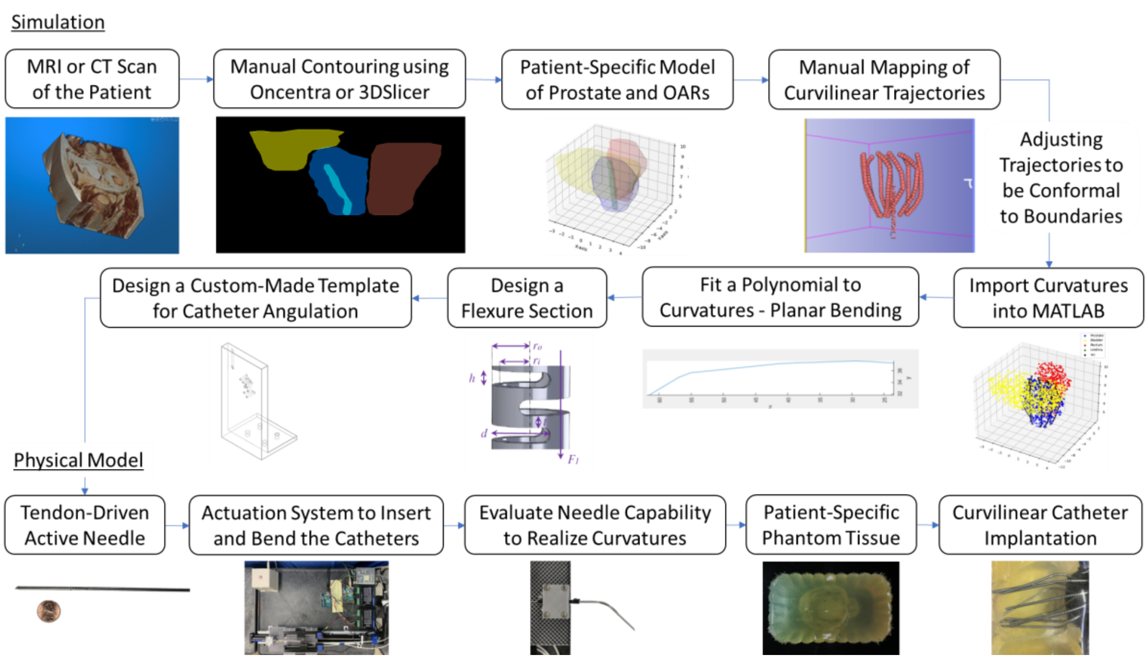

Figure 1. A framework to realize the curvilinear catheter implantation for optimized HDR BT.

2.1. Curvilinear catheter implantation

This section presents methods to preplan a curvilinear catheter configuration conformal to the patient-specific anatomy followed by a dose plan.

2.1.1. Preplanning needle configuration for an anonymized patient

T2-weigthed MRIs of an anonymized patient from our practice were first obtained. The prostate, and the OARs, i.e., urethra, rectum, and bladder were then manually contoured (Figure 2a) to construct 3D model of the patient-specific organs. The 3D models (volumes) of the organs were then exported as STL files for further analysis. Curved trajectories were manually mapped inside the prostate gland, conformal to the prostate capsule, closer to the peripheral zone of the prostate, and away from the OARs. Using Oncentra HDR TPS and HIPO optimizer, a dosimetric plan was generated using curvilinear catheters that overlayed on the curved trajectories. The plan generated ten curved catheters, as shown in Figure 2b, to host the radiation source for treatment.

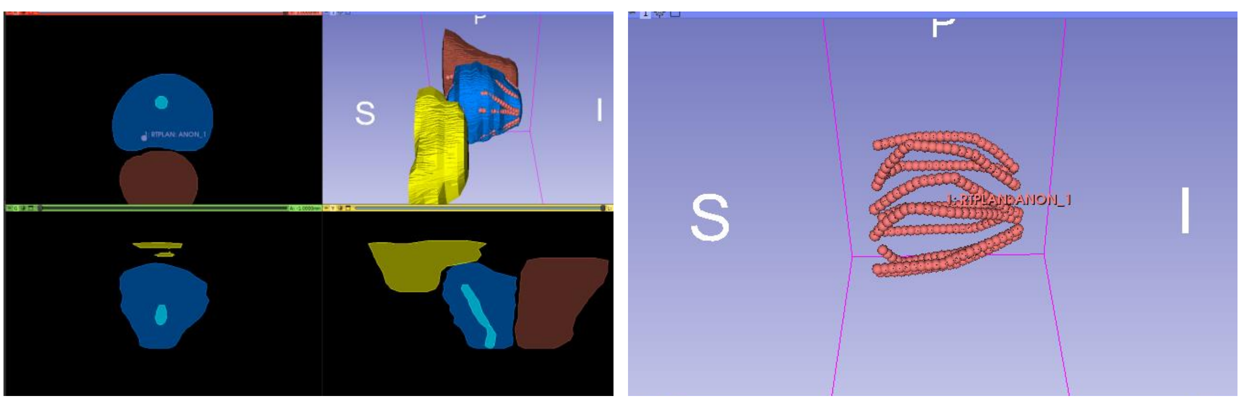

(a) (b)

Figure 2. (a) Contours of prostate, urethra, bladder, and rectum to identify and model the organs, (b) ten curved trajectories mapped inside prostate gland conformal to the boundaries for curvilinear catheter implantation.

2.1.2. Dosimetric evaluation of the plan with curvilinear catheter implantation

Dwell positions and dwell time for the radiation source were planned using Oncentra software based on the dose prescription for the anonymized patient. Data were collected for D_{90}, V_{100}, V_{150}, V_{200}; for prostate (target); D_{max}, D_{2cc}, V_{12Gy}; for rectum; D_{max}, D_{10}, V_{100}, for urethra, and D_{max} for bladder from dose-volume histogram (DVH) were collected. Section 3.1 describes the dosimetric benefits of the curvilinear catheter implantation.

2.2. Tendon-driven active needles

2.2.1. Curvature analyses – 2D planar bending

The curved trajectories, generated in the previous step using Oncentra, were imported into MATLAB as 3D coordinate text files, identifying several points along their trajectories (see Figure 2b). The trajectories displayed curvatures in different planes. To represent each trajectory as a 2D planar curvature, a second order polynomial was fitted to the data points. Table 1 lists the catheters with the best fit polynomial, the radius of curvature (R), and the curvature (K) for the ten trajectories. The average, maximum, and minimum radius of curvature (R) for all ten catheters were 56.48, 165.50, 15.19mm, respectively, with a standard deviation of 44.55mm. The average, maximum, and minimum curvature (K) for all ten catheters were 0.03, 0.07, 0.01 mm^{-1}, respectively, with a standard deviation of $0.02mm^{-1}$, covering a wide range of curvatures for the catheters. The average, maximum, and minimum bending angle of all ten catheters were 22.36, 49.99, 4.59 deg, respectively, with a standard deviation of 16.41 deg.

Table 1. Polynomial fit to the curvilinear catheters preplanned using Oncentra.

Catheter	x^2	x	*int*	Radius of Curvature *R* (mm)	Curvature, *K*, *1/R* (1/mm)	Angular bending (deg)
1	-0.0067	0.4567	30.0045	74.42	0.01	10.21
2	-0.0094	0.7743	21.8162	53.10	0.02	14.30
3	-0.0030	0.2478	30.5477	165.50	0.01	4.59
4	-0.0142	1.3510	-13.8872	35.21	0.03	21.57
5	0.0114	-1.1749	12.8432	43.67	0.02	17.39
6	-0.0329	2.9523	-44.2359	15.19	0.07	49.99
7	0.0076	-0.9477	15.6304	65.46	0.02	11.60
8	0.0067	-0.7836	32.1606	75.18	0.01	10.10
9	-0.0317	2.8600	-46.9309	15.80	0.06	48.09
10	-0.0235	2.1377	-36.6467	21.28	0.05	35.70

2.2.2. Tendon-driven active needle design to realize required curvatures

Tendon-driven active needles have been used to bend inside tissue for path tracking and accurate targeting in different applications [8–10]. The tendon-driven active needle features a flexure section (Figure 3a) inclusive to several notches that are carved on the needle's Nitinol tube for improved flexibility. The flexure section is actuated via two internal tendons, shown in the figure, for bidirectional planar bending. The length of the flexure section as well as the height and depth of the notches and the number of notches could alternate to facilitate different curvatures (angular bending). The tendon-driven active needle and the angular bending are shown in Figure 3b. The flexure section of the active needle is insulated using a biocompatible and ultrathin (wall thickness of 76μm) medical-grade heat shrink tubing to prevent tissue penetration inside the needle tube.

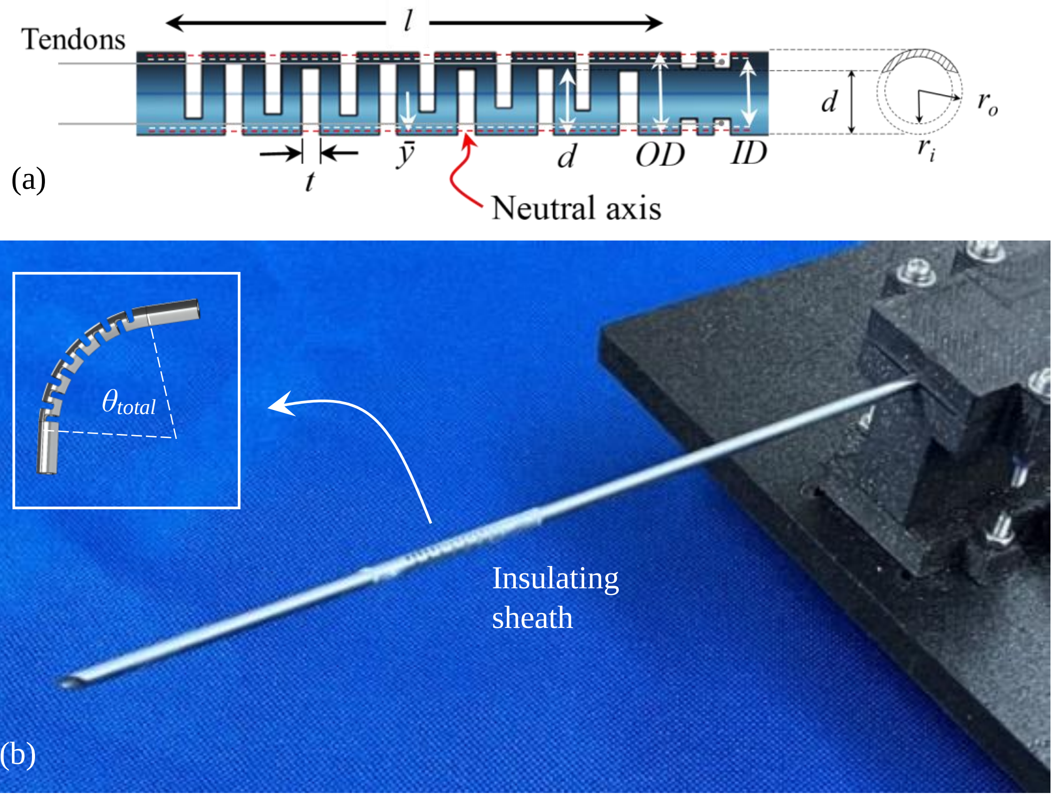

Figure 3. (a) Flexure section of the tendon-driven active needle, and (b) the fabricated prototype with an insulating sheath.

The following equations are used to estimate the bending angle (and consequently the radius of curvature) of the flexure section. For the notches schematically shown in Figure 3a, the neutral bending axis can be calculated using the following equation [11]:

$$\bar{y} = \frac{4({r_o}^3 \, sin^3(\phi_o) - {r_i}^3 \, sin^3(\phi_i))}{3\left({r_o}^2(2\phi_o - sin\, 2\,\phi_o) - {r_i}^2(2\phi_i - sin\, 2\,\phi_i)\right)} \quad (1)$$

$$r_i = \frac{ID}{2}, r_o = \frac{OD}{2} \qquad (2)$$

where $\bar{y}$ is the distance moved from the center of the tube, *OD*, *ID*, r_o, and r_i are the outer and inner diameters, outer and inner radii of the needle tube, respectively, and ϕ_o and ϕ_i are found by the following equations:

$$\phi_o = arccos(\frac{d - r_o}{r_o}) \quad (3)$$

$$\phi_i = arccos(\frac{d - r_o}{r_i}) \quad (4)$$

where *d* is the notch depth. The bending angle for each notch can be estimated as:

$$\theta_i = \frac{h}{r_o + \bar{y}} \quad (5)$$

where *h* is the height of the neutral axis for each, which in this work is equal to the height of the cut (*t*).

The flexure section of the active needle was designed for the smallest radius of curvature among the ten catheters listed in Table 1 (i.e., Catheter 3). The bending angle for the sharpest curved trajectory was 50.11 degrees.

Assuming that the total deflection is distributed equally among the notches, the bending angle of the whole flexible section (θ_{total}) could be found by multiplying the bending angle of each notch (θ_i) by the number of notches.

Table 2. The dimensions of the notches for the active needle. Units are in mm.

l	$r_i\ (ID)$	$r_o\ (OD)$	$\bar{y}$	d	t
13.280	0.745 (1.49)	0.965 (1.93)	1.450	1.680	0.460

Dimensions of each notch for the active needles are listed in Table 2. Using the equations above, the angular deflection of each notch was 14.76 degrees. The overall angular deflection of the flexure sections (eight notches) 118.08 degrees, which surpasses the required angular deflection of 50.11 degrees for the active needle.

Next section evaluates the capability of the tendon-driven active needle, with the dimensions shown in Figure 3 and listed in Table 2, to realize the required curvatures listed in Table 1.

2.2.3. Tendon actuation to curve needles - bending evaluations in air

The needle insertion and actuation system, shown in Figure 4, was used to push the needle forward and to pull the tendons to realize the curvatures on each catheter. The system consists of stepper motors, gear boxes, and lead screws to insert and bend the catheters for proper implantation inside prostate. The motors were programmed to pull the internal tendons. The experimental setup for automated control of the robotic tool consists of two NEMA 11 stepper motors (ToAuto, Shenzhen, China) attached to two 100mm linear rails. Each motor is attached to one tendon that is responsible for tightening or loosening the tendons to perpetuate bending at the active needle. The motors are wired to DM542T drivers (StepperOnline Inc., New York, NY), which are run through Arduino Uno control boards. Serial communications are established between the Arduino boards and a Python script on a computer to control the tendon displacement.

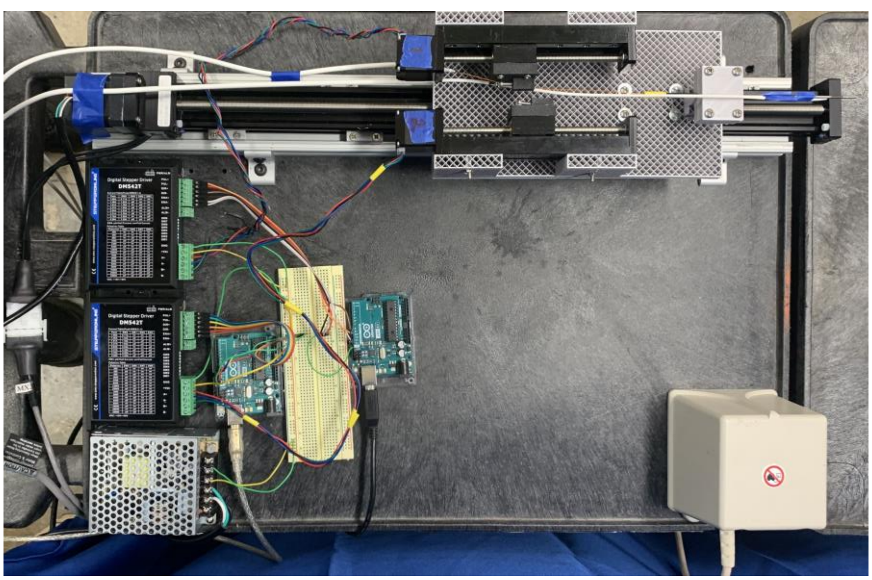

Figure 4. Needle insertion and actuation system to push the needle forward and bend the needle to realize curvatures.

2.3. Feasibility study

This section demonstrates the feasibility of using tendon-driven active needles to realize a curvilinear catheter implantation in phantom tissues.

2.3.1. Patient-specific phantom tissue

An injection molding process was used here to develop a patient-specific phantom tissue. The mold (Figure 5a) was designed using the prostate model (Figure 5b), extracted from the MRI of the patient, to make a real scale phantom. Plastic softener and hardener were injected into the mold, solidified, and extracted to form a prostate-shaped phantom. The prostate-shaped phantom was then embedded inside a larger phantom (Figure 5c) for catheter implantation. Figure 5d is the ultrasound image of the phantom tissue showing the boundaries of the patient's prostate.

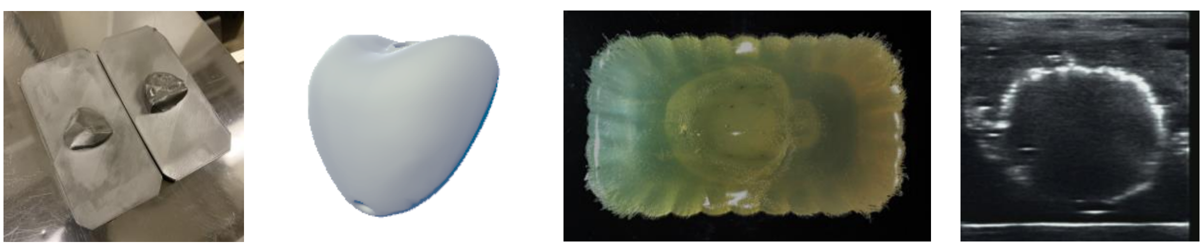

(a) (b) (c) (d)

Figure 5. Patient-specific phantom tissue developed using (a) injection molding, where the mold was made using (b) the 3D model of the patient's prostate, (c) embedded inside a larger phantom, with (d) the ultrasound image for catheter implantation.

2.3.2. Curvilinear implantation inside a patient-specific phantom tissue

The actuation system, described in Section 2.2.3 was used to insert and bend the catheters sequentially inside the patient-specific phantom tissue explained in Section 2.3.1. A clamp was designed, and 3D printed to secure the tendons and keep the needles' curvatures inside the prostate.

3. Results

3.1. Improved dosimetric plans via curvilinear catheter implantation

This section evaluates dosimetric benefits when HDR BT is performed using curvilinear catheter implantation. An additional dose plan was generated using conventional rectilinear catheter implantation method for direct comparison with the plan generated Section 2.1.1. Table 3 lists the dosimtric data for the two plans generated with curvilinear as well as rectilinear catheter implantation. The rectilinear catheter implantation failed to meet the dose constraint for the rectum (12Gy < 0.6cc), while satisfactory with the curvilinear catheter implantation. The number of needles required to meet the dosimetric constraints for the prostate (target) and the OARs (urethra, rectum, and bladder) was significantly lower (22 vs. 10 catheters) for the curvilinear compared to the rectilinear catheter implantation approach.

Table 3. Dosimetric plan using curvilinear and rectilinear catheter implantation.

Curvilinear catheter implantation

Prostate					Urethra				
vol (cc)	*D_{90} (Gy)*	*V_{100} (%)*	*V_{150} (%)*	*V_{200} (%)*	*D_{10} (Gy)*	*D_{10} (% Rx)*	*V_{100} (%)*	*Max dose (cGy)*	*Max (% Rx)*
64.8	16.2	95.2	37.3	13.8	18.0	119.9%	92.3	18.4	122.7%

Rectum			Bladder	Needles
Vol of 12 Gy (cc)	*$D_{\_2cc}$ (cGy)*	*Max Dose (cGy)*	*Max Dose (cGy)*	*Curved*
0.54	10.9	13.3	18.4	10

Rectilinear catheter implantation

Prostate					Urethra				
vol (cc)	*D_{90} (Gy)*	*V_{100} (%)*	*V_{150} (%)*	*V_{200} (%)*	*D_{10} (Gy)*	*D_{10} (% Rx)*	*V_{100} (%)*	*Max dose (cGy)*	*Max (% Rx)*
64.8	16.0	95.6	29.8	11.1	17.8	118.6%	92.3	18.3	122.2%

Rectum			Bladder	Needles
Vol of 12 Gy (cc)	*$D_{\_2cc}$ (cGy)*	*Max Dose (cGy)*	*Max Dose (cGy)*	*Straight*
0.90	11.2	13.4	19.9	22

Figure 6 shows the heat map of the prostate due to the radiation received in HDR BT when the radiation source is positions inside the curvilinear catheters along with the DVH diagram. Using this method, larger dose has been delivered to the peripheral zone of the prostate, where the cancer is normally located.

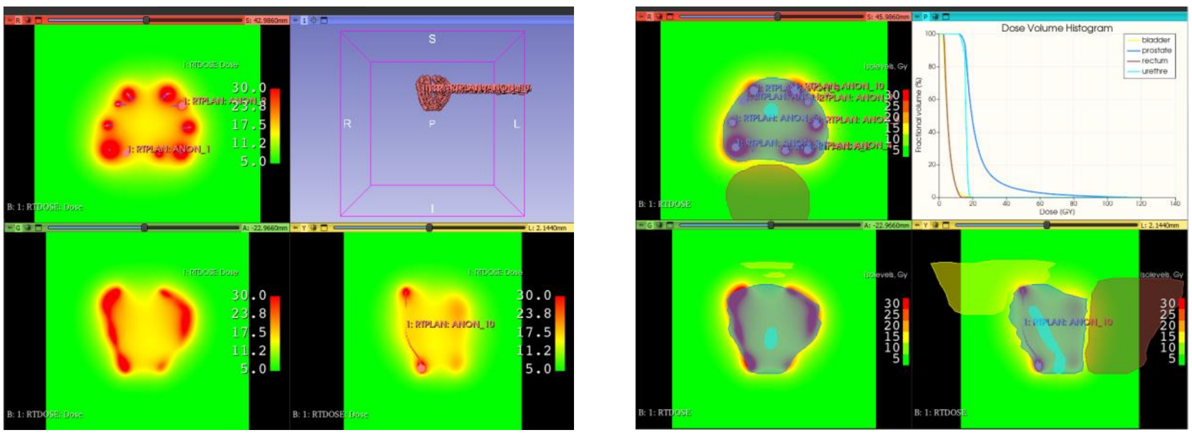

(a) (b)

Figure 6. Radiation heat map: (a) dose distribution inside the prostate gland, and (b) dose volume histogram (DVH).

3.2. Curvature demonstration and evaluations in air

The curvatures of the ten catheters, listed in Table 1, were realized by the tendon-driven active needles using the actuation system shown in Figure 4. The curvatures were 3D printed and placed behind the bent catheters for visual comparison.

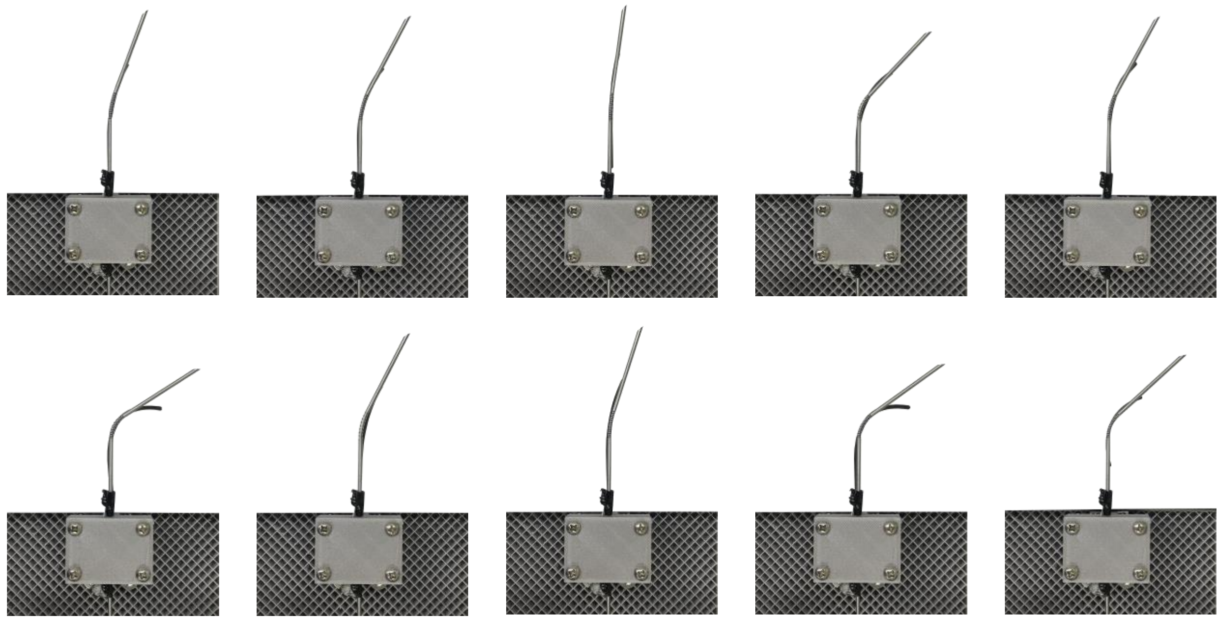

Figure 7. Tendon-driven active needles actuated to realize the desired curvatures of the curved trajectories as planned in Section 2.2.1. Top and bottom row, left to right correcponds to Catheters 1 to 10 from Table 1. The required curvatures are 3D printed in black color and placed behind the active needle for visual comparison.

The capability of the active needle, presented in Section 2.2.2, to realize desired curvatures in air was evaluated by directly comparing the simulated curvatures with the curvatures of the active needles realized upon actuation. Table 4 lists the simulated and the actual radii of curvature and bending angles of the catheters resulted from curve fitting and realized by the active needles, respectively. The deviations from the desired radii of curvature and the bending angles were estimated and the errors were reported. The average error in realizing the desired radius of curvature and the bending angle was 18.28 and 24.55%, respectively. Larger errors are associated with the dimensions of the flexure section of the active needle (e.g., length of the section, depth and height of each notch, and the number of notches) that are not designed for a specific desired curvature. Improved accuracy could be achieved by designing a few active needles with different flexure sections to cover the wide range of desired curvatures (which was the case in this work).

The active needle, presented in this work, was able to represent most of the desired curvatures with reasonable accuracy.

Table 4. Simulated and realized radius of curvature and bending angle of the active needles shown in Figure 7. Units are mm and deg for radii of curvature and bending angles, respectively.

Radius of curvature (simulation)	Bending angle (simulation)	Radius of curvature (actual)	Bending angle (actual)	Error in realizing radius of curvature (%)	Error in realizing bending angle (%)
74.42	10.21	64.10	11.85	13.86	16.09
53.10	14.30	44.64	17.01	15.93	18.95
165.50	4.59	192.31	3.95	16.19	13.94
35.21	21.57	20.83	36.46	40.83	69.01
43.67	17.39	43.86	17.32	0.43	0.43
15.19	49.99	10.96	69.27	27.83	38.56
65.46	11.60	47.17	16.10	27.94	38.77
75.18	10.10	75.76	10.03	0.77	0.76
15.80	48.09	13.30	57.12	15.81	18.79
21.28	35.70	16.34	46.48	23.20	30.21

The tendon pulling force of the active needle was estimated using the equation below for the lead screw [12],

$$T = \frac{F_p d_m}{2} \left(\frac{l + \pi f d_m sec\alpha}{\pi d_m - f l sec\alpha}\right) \qquad (6)$$

where T is the applied torque by the Maxon motor to pull the tendons, d_m is the mean diameter of a single thread lead screw, F_p is the tendon pulling force to be found, l is the tendon displacement, f is the coefficient of friction for threaded pairs of a steel and dry screw, which is 0.25 here, and α is the thread angle, which is zero for a square thread [12].

The applied torque (T) was estimated using the motor's current, nominal current, and torque constant using the following equations.

$$\text{Torque actual value (per mil)} = \frac{Current\ (mA)}{\text{Nominal current (mA)}} * 1000 \tag{7}$$

$$T\ (mNm) = \left(\frac{\text{Torque actual value (per mil)}}{1000}\right) * \left(\frac{Nominal\ current}{1000}\right) * Torque\ constant\ (mNm/A) \tag{8}$$

To find the bending angle θ in each step of insertion, the following equation could be use,

$$\theta = \tan^{-1}\frac{u_t(i) - u_t(0)}{z(i) - z(0)} \tag{9}$$

where $u_t(i)$ and $u_t(0)$ are the needle tip paths at moment i and at the initial moment, respectively, and $z(i)$ and $z(0)$ are the insertion depths at moment i and at the initial moment, respectively.

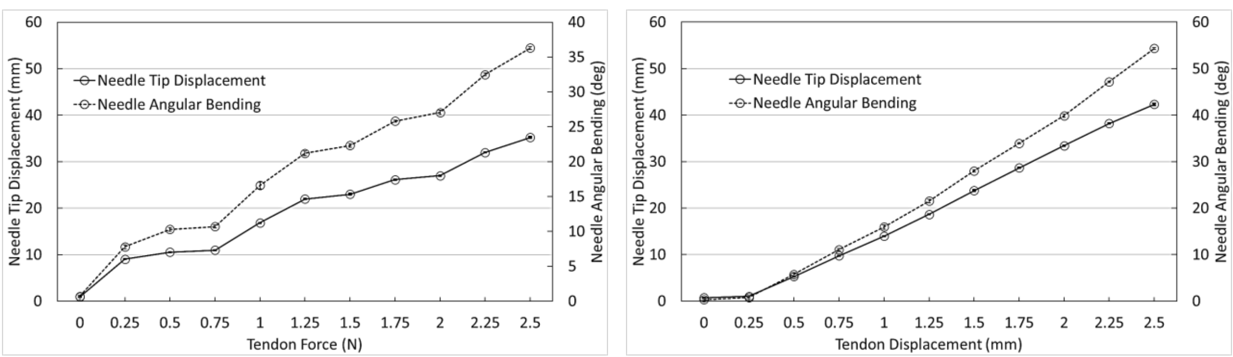

(a) (b)

Figure 8. Tip displacement and angular bending of the tendon-driven active needle via (a) tendon displacement, and (b) tendon force actuations.

Figures 8a and 8b show the needle tip displacement and angular bending with respect to tendon displacement and tendon pulling force, respectively. Figure 9 shows the needle tip displacement, radius of curvature, and angular bending of the tendon-driven active needle via tendon displacement actuation using the actuation system (Figure 4) for the ten catheters planned for curvilinear implantation (listed in Table 1).

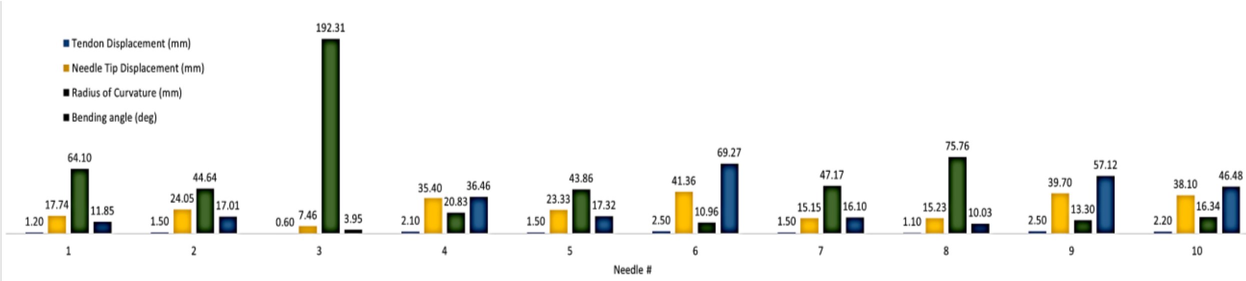

Figure 9. Tendon displacement, needle tip displacement, radius of curvature, and angular bending for the ten catheters listed in Table 1, realize by the tendon-driven prototype and the actuation system.

A custom-made template (shown in Figure 10) was designed and fabricated to properly angulate the catheters. Insertion angles of the catheters are defined on the template to facilitate insertion and bending conformal to the prostate gland boundaries. Figure 10a and 10b demonstrate curvilinear catheter implantation consisting of the ten catheters planned previously in Section 2.1.1. The tendons were pulled using the actuation system, and then secured using 3D clamps, to keep the desired curvatures. The tendons were actuated sequentially using the same actuation system.

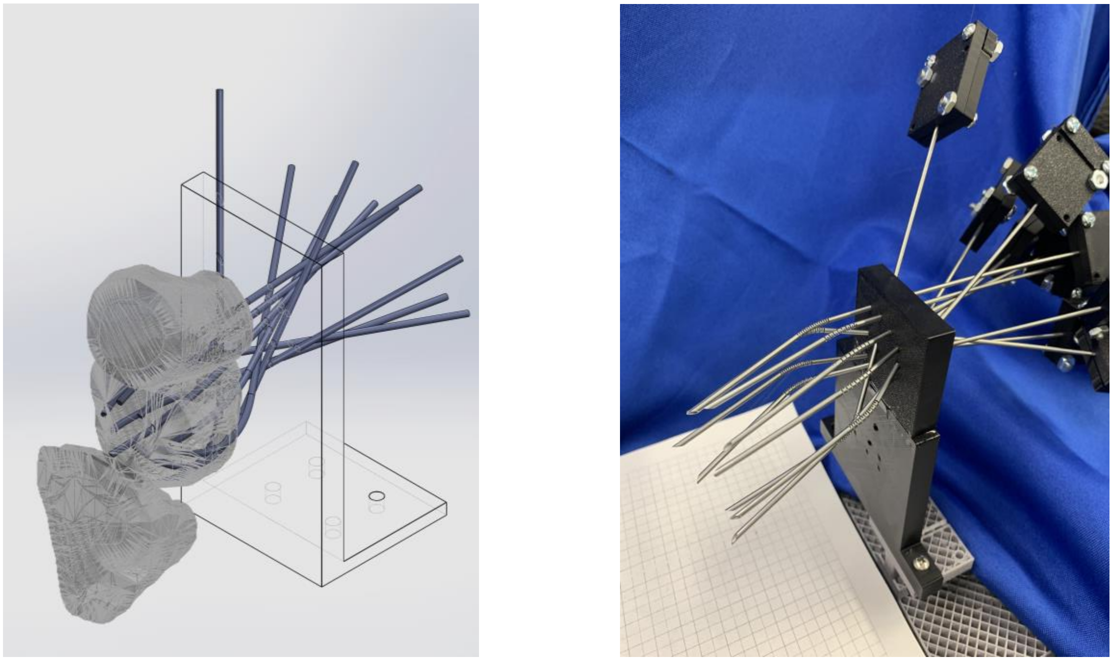

(a) (b)

Figure 10. Curvilinear catheter implantation: (a) 3D model of the assembly, and (b) configuration demonstrated in air.

3.3. Evaluating curvilinear catheter implantation in patient-specific phantom tissue

The tendon-driven active needles were inserted into the phantom tissue using the actuation system. The active needles were gradually inserted and bent inside the phantom to realize the required curvatures. Figure 11a shows the catheters implanted inside the phantom conformal to the prostate boundaries. A transverse ultrasound image was obtained to show the position of all ten curvilinear catheters inside the phantom tissue. The cross section of the catheters appears in the ultrasound image, as marked in the figure with red circles.

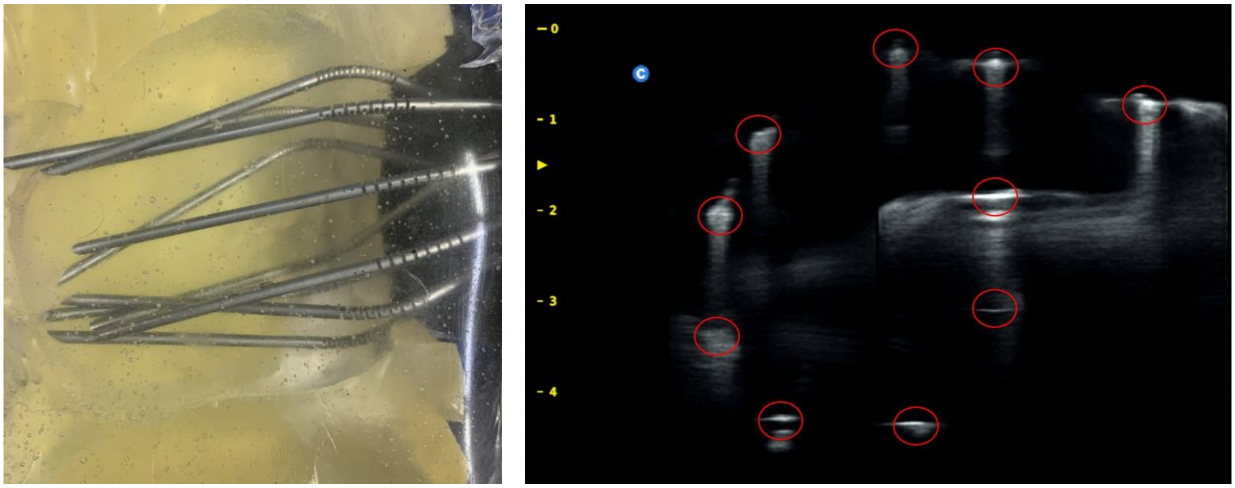

(a) (b)

Figure 11. Curvilinear catheter implantation: (a) inside a patient-specific phantom tissue, and (b) transverse ultrasound image of the implant showing the position of all catheters in red circles.

4. Discussion

This work introduces curvilinear catheter implantation approach to replace the conventional rectilinear catheter implantation method in prostate HDR brachytherapy. The curvilinear catheter implantation improves dosimetric plans inclusion coverage to the prostate (target) as well as dose constraints to the OARs (urethra, rectum, and bladder), with a substantial reduction in number of needles. Specifically designed and developed tendon-driven active needles were used to curve inside the prostate to facilitate curvilinear catheter implantation. The flexure section of the active needle was designed based on the required curvatures to conform to the patient-specific anatomy. A curvilinear catheter implantation was then demostrated using the active needles (operated robotically using an actuation system) in air and inside a patient-specific phantom tissue to show the feasibility of this approach.

This work concludes that tendon-driven active needles could specifically designed and developed to replace conventional straight needles in HDR prostate BT, enabling curvilinear catheter implantation with improved conformity to the patient's specific anatomy. Arrangement of the curvilinear catheters closer to the areas of interests provides unique opportunity for dose escalation to the dominant intraprostatic lesions.

Any imprecision in curvilinear catheter implantation (if exists) is compensated at the replanning stage of HDR BT procedure after actual implantation of the catheters and using actual positions of the catheters inside the prostate (obtained by additional CT scan).

5. Acknowledgement

Research reported in this publication was supported by the National Institute Of Biomedical Imaging And Bioengineering of the National Institutes of Health under Award Number K25EB030562. The content is solely the responsibility of the authors and does not necessarily represent the official views of the National Institutes of Health.

6. References

[1] 2023, "American Cancer Society (ACS), Cancer Statistics Center" [Online]. Available: https://cancerstatisticscenter.cancer.org/?_ga=1.176033250.196666305.1484171292#!/.

[2] Yoshioka, Y., Yoshida, K., Yamazaki, H., Nonomura, N., and Ogawa, K., 2013, "The Emerging Role of High-Dose-Rate (HDR) Brachytherapy as Monotherapy for Prostate Cancer," J. Radiat. Res., **54**(5), pp. 781–788.

[3] Challapalli, A., Jones, E., Harvey, C., Hellawell, G. O., and Mangar, S. A., 2012, "High Dose Rate Prostate Brachytherapy: An Overview of the Rationale, Experience and Emerging Applications in the Treatment of Prostate Cancer," Br. J. Radiol., **85**(SPEC. ISSUE 1).

[4] Zelefsky, M. J., Yamada, Y., Cohen, G., Venkatraman, E. S., Fung, A. Y., Furhang, E., Silvern, D., and Zaider, M., 2000, "Postimplantation Dosimetric Analysis of Permanent Transperineal Prostate Implantation: Improved Dose Distributions with an Intraoperative Computer-Optimized Conformal Planning Technique," Int. J. Radiat. Oncol. Biol. Phys., **48**(2), pp. 601–608.

[5] Crook, J., Ots, A., Gaztañaga, M., Schmid, M., Araujo, C., Hilts, M., Batchelar, D., Parker, B., Bachand, F., and Milette, M. P., 2014, "Ultrasound-Planned High-Dose-Rate Prostate Brachytherapy: Dose Painting to the Dominant Intraprostatic Lesion," Brachytherapy, **13**(5), pp. 433–441.

[6] Schick, U., Popowski, Y., Nouet, P., Bieri, S., Rouzaud, M., Khan, H., Weber, D. C., and Miralbell, R., 2011, "High-Dose-Rate Brachytherapy Boost to the Dominant Intra-Prostatic Tumor Region: Hemi-Irradiation of Prostate Cancer," Prostate, **71**(12), pp. 1309–1316.

[7] Podder, R., Zheng, Y., Konh, B., Lyons, K., Biswas, T., Ove, R., Traughber, B., and Podder, T., 2023, "Curvilinear-Needle Implantation: A New Technique for Prostate HDR Brachytherapy," *AAPM 65th Annual Meeting & Exhibition*.

[8] Padasdao, B., Lafreniere, S., Rabiei, M., Batsaikhan, Z., and Konh, B., 2023, "Teleoperated and Automated Control of a Robotic Tool for Targeted Prostate Biopsy," Jounral Med. Robot. Res., **8**(1&2), p. 2340002.

[9] Konh, B., Padasdao, B., Batsaikhan, Z., and Ko, S. Y., 2021, "Integrating Robot-assisted Ultrasound Tracking and 3D Needle Shape Prediction for Real-time Tracking of the Needle Tip in Needle Steering Procedures," Int. J. Med. Robot. Comput. Assist. Surg.,

17(4), p. e2272.

[10] Padasdao, B., Varnamkhasti, Z. K., and Konh, B., 2020, "3D Steerable Biopsy Needle with a Motorized Manipulation System and Ultrasound Tracking to Navigate inside Tissue," J. Med. Robot. Res., **5**(03n04), p. 2150003.

[11] Eastwood, K. W., Francis, P., Azimian, H., Swarup, A., Looi, T., Drake, J. M., and Naguib, H. E., 2018, "Design of a Contact-Aided Compliant Notched-Tube Joint for Surgical Manipulation in Confined Workspaces," J. Mech. Robot., **10**(1), pp. 1–12.

[12] Budynas, R. G., Nisbett, J. K., and Shigley, J. E., 2018, *Shigley's Mechanical Engineering Design*.

7. List of Figures

Figure 1. Framework to realize a curvilinear catheter implantation for optimized HDR BT.

Figure 2. (a) Contouring prostate, urethra, bladder, and rectum to identify and model the organs, (b) ten curved trajectories mapped inside prostate gland conformal to the boundaries for curvilinear catheter implantation.

Figure 3. (a) Flexure section of the tendon-driven active needle, and (b) the fabricated prototype with an insulating sheath.

Figure 4. Needle insertion and actuation system to push the needle forward and bend the needle to realize curvatures.

Figure 5. Patient-specific phantom tissue developed using (a) injection molding, where the mold was made using (b) the 3D model of the patient's prostate, (c) embedded inside a larger phantom, with (d) the ultrasound image for catheter implantation.

Figure 6. Radiation heat map: (a) grey scale inside the prostate gland, and (b) dose volume histogram (DVH).

Figure 7. Tendon-driven active needles actuated to realize the required curvatures of the curved trajectories as planned in Section 2.2.1 – Top and bottom row, left to right correcponds to Catheters 1 to 10 from Table 1. The required curvatures are 3D printed in black color and placed behind the active needle for visual comparison.

Figure 8. Tip displacement and angular bending of the tendon-driven active needle via (a) tendon displacement, and (b) tendon force actuations.

Figure 9. Tendon displacement, needle tip displacement, radius of curvature, and angular bending for the ten catheters listed in Table 1, realize by the tendon-driven prototype and the actuation system.

Figure 10. Curvilinear catheter implantation: (a) 3D model of the assembly, and (b) configuration demonstrated in air.

Figure 11. Curvilinear catheter implantation: (a) inside a patient-specific phantom tissue, and (b) transverse ultrasound image of the implant showing the position of all catheters in red circles.

8. List of Tables